Polymer Chemistry

ROYAL SOCIETY OF CHEMISTRY

PAPER

View Article Online
View Journal

Check for updates

Cite this: DOI: 10.1039/d1py01442k

Highly tunable metal-free ring opening polymerization of glycidol into various controlled topologies catalyzed by frustrated lewis pairs†

Si Eun Kim,[a,b] Yu-Ri Lee,[c] Minseong Kim,[d,e] Eunyong Seo,[a,f] Hyun-Jong Paik,[b] Jin Chul Kim,[a] Ji-Eun Jeong,[a] Young Il Park,*[a] Byeong-Su Kim*[d] and Sang-Ho Lee*[a]

Received 28th October 2021,
Accepted 24th January 2022

DOI: 10.1039/d1py01442k

rsc.li/polymers

Controlling the topology of a polymer is essential in determining its physical properties and processing. Even after numerous studies, obtaining a diverse array of topologies, particularly within the framework of hyperbranched systems, remains challenging. Here, we propose a synthetic approach to obtain highly tunable hyperbranched polyglycidol (hb-PG) using a frustrated Lewis pair of pyridine or tributylamine along with tris(pentafluorophenyl)borane, $B(C_6F_5)_3$, that not only influences the preferred activated monomer mechanism through hydrogen bonding with the glycidol monomer, but also facilitates the formation of unique polymer topologies. Notably, the frustrated Lewis pair containing pyridine was found to yield a branched polymer carrying cyclic structures (branched cyclic polymers) with an increased degree of branching, whereas the more sterically hindered tributylamine yielded hb-PG without a cyclic structure; these results were confirmed by MALDI-ToF analyses. Based on the unique topologies of the PGs, significant correlations between the topology and the bulk and solution states were investigated using SEC, DSC, and ^{1}H NMR diffusion-ordered spectroscopy.

Published on 26 January 2022. Downloaded by Yonsei University on 2/28/2022 1:44:30 AM.

Introduction

Over the past few decades, the design of polymer topologies with unique properties and functions in the bulk and solution states has led to challenges in the development of novel synthesis strategies in polymer science and technology.[1,2] Dendrimers,[3–5] graft polymers,[6,7] hyperbranched polymers,[8,9] and macrocyclic polymers[10,11] are examples of remarkable polymer architectures. Among them, dendritic macromolecules have attracted considerable attention because of their large number of functional groups along with interesting physical features, even though they are synthesized through effort-intensive routes. Alternatively, hyperbranched polymers, which are an intermediate form between linear polymers and dendrimers, have been widely investigated due to their relatively simple synthetic access to various degrees of branching. Moreover, unlike their linear analogues, macrocyclic polymers show promise for use in unique applications due to the absence of polymeric chain ends.[11] Despite the numerous active studies detailing small structural differences in polymeric topologies, achieving a diverse array of topologies, particularly within a framework of hyperbranched systems, remains underexplored.

As a representative example of topologically controlled polymers, hyperbranched polyglycidols (hb-PGs) have widely attracted intensive attention because of their unique three-dimensional architecture that comprises a highly flexible polyether backbone with multiple functional hydroxyl groups and their excellent biocompatibility.[12] In particular, commercially available and reactively functional glycidol as a latent AB_2-type monomer yields hb-PG in a single step.[13,14] Recent synthesis efforts have been focused on developing well-defined and complex architectures of homo- and copolymers of PGs with various molecular weights, functionalities, and structures.[15–17] Although other parameters of macromolecules are also important, the degree of branching (DB) in hyperbranched polymers is especially relevant because it determines the precise microstructures of the resulting polymers.[18–20]

[a]Center for Advanced Specialty Chemicals, Korea Research Institute of Chemical Technology, Ulsan 44412, Republic of Korea
[b]Department of Polymer Science and Engineering, Pusan National University, Busan 46241, Republic of Korea
[c]Materials Architecturing Research Center, Korea Institute of Science and Technology, Seoul 02792, Republic of Korea
[d]Department of Chemistry, Yonsei University, Seoul 03722, Republic of Korea. E-mail: bskim19@yonsei.ac.kr
[e]Department of Chemistry, Ulsan National Institute of Science and Technology (UNIST), Ulsan 44919, Republic of Korea
[f]Department of Chemical Engineering, Ulsan College, Ulsan 44610, Republic of Korea
†Electronic supplementary information (ESI) available. See DOI: 10.1039/d1py01442k

Published on 26 January 2022. Downloaded by Yonsei University on 2/28/2022 1:44:30 AM.

Recently, new synthetic approaches that enable control of the PG architecture and the DB using novel catalysts[21] or functional monomers[22] have been reported. For example, Haag's group reported using citric acid as a proton donor and an activating agent for cationic ring-opening polymerization (CROP) to generate hb-PG.[23] In addition, Kim *et al.* reported the preparation of hb-PG using a double metal cyanide catalyst that promotes an active chain end (ACE) mechanism by coordinating between the glycidol monomer and the catalyst.[24] In another notable effort, Harth *et al.* reported the preparation of semi-branched PG with a low branching density using a phosphate buffer solution.[25] Interestingly, Bujans's group demonstrated tris(pentafluorophenyl)borane ($B(C_6F_5)_3$, BCF)-catalyzed zwitterionic ring-opening polymerization of oxirane monomers to provide cyclic polyethers through a simple reaction.[26] Recently, we have reported a recyclable metal-free catalytic system for the CROP of glycidol under ambient conditions.[27] Here, the $B(C_6F_5)_3$ catalyst is tolerant to air and humidity, which allows its application in CROP using unpurified reagents under ambient conditions. Particularly, the growing PG chains in nonpolar solvents can be automatically separated because of their increased molecular weight and hydrophilicity, which causes phase separation that yields a uniform molecular weight of the resulting PGs. Therefore, the recycling polymerization was successfully performed through repetitive decantation along with addition of an unpurified monomer. Although successful control of polymer topologies can be achieved in hyperbranched polymers, an effective polymerization procedure with a tunable DB that can enhance the polymerization yield and the purity of products is still highly desirable.

Frustrated Lewis pairs (FLPs) that combine a Lewis acid with a base exhibiting steric hindrance have recently been demonstrated to enhance the reactivity of cyclic ester monomers and polar vinyl monomers during polymerization.[28–30] For example, Li *et al.* have reported the ring-opening polymerization of lactide using $Zn(C_6F_5)_2$ along with organic Lewis bases to form a cyclic polyester.[31] Moreover, FLPs have been applied in living cationic polymerizations to ensure high reactivity in the system caused by the dissociation and recombination of the Lewis acid and base, which function as the inactive dormant species (Lewis adduct) and the active propagating species (dissociated Lewis pair or the FLPs).[32–34] However, the successful application of Lewis pairs in the ring-opening polymerization of oxirane-based monomers is still rare.

Herein, we report the metal-free ring opening polymerization of glycidol to generate a diverse array of hyperbranched and branched cyclic PGs with precise control of their topologies (Scheme 1). The FLPs formed here between $B(C_6F_5)_3$ and Lewis bases such as tributylamine (TBA) and pyridine (Py) can tailor the topologies of the polymers depending on the bulkiness of the Lewis bases. Moreover, we also demonstrated that

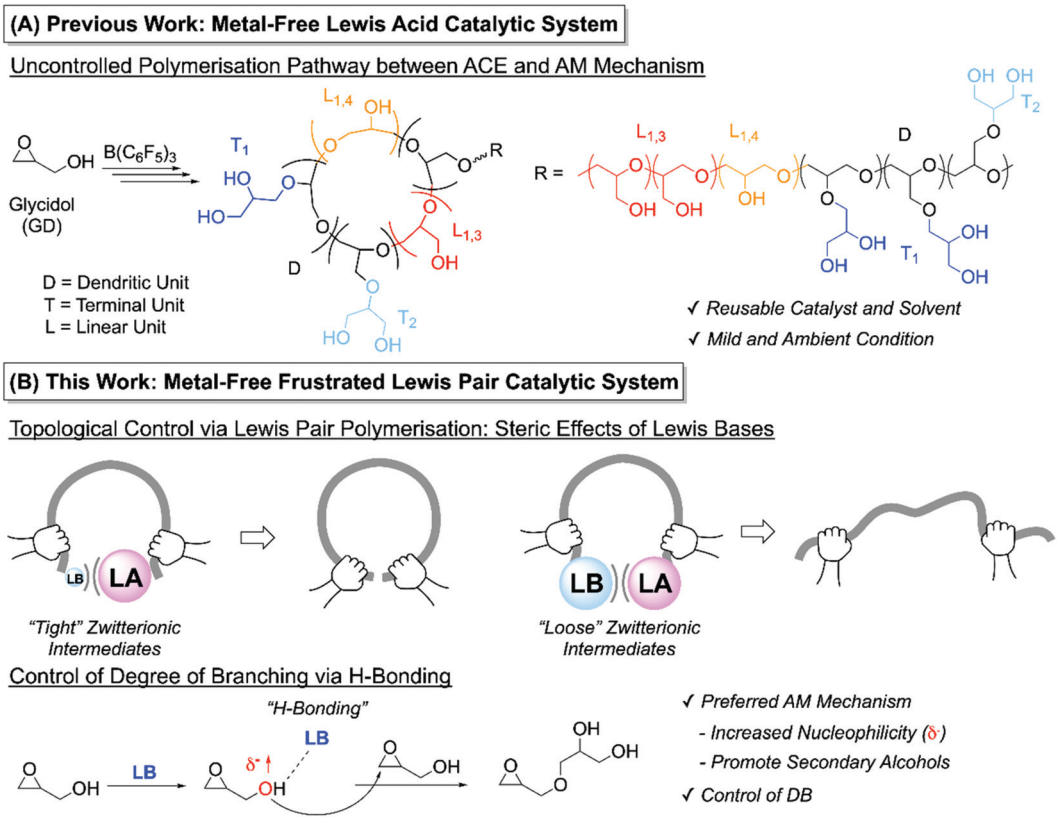

Scheme 1 Metal-free cationic ring opening polymerization using (A) pure Lewis acid catalytic system and (B) FLP catalytic system.

 This journal is © The Royal Society of Chemistry 2022

Published on 26 January 2022. Downloaded by Yonsei University on 2/28/2022 1:44:30 AM.

competition between the ACE and the activated monomer (AM) mechanisms influences the DB, thereby affecting the microstructures of the PGs. Specifically, the added Lewis base interacts with the hydroxyl group of glycidol through hydrogen bonding (H-bonding), thereby increasing the nucleophilicity of the oxygen in the hydroxyl group that drives the preference for the AM mechanism (Scheme 1B). Furthermore, the relative concentration of the glycidol monomer will decrease during polymerization, whereas the concentration of hydroxyl groups will remain almost constant, which would affect the degree of branching in the polymer chain *via* the preferred AM mechanism. Based on these unique PG topologies with well-defined structures, significant correlations between the topology and the bulk and solution states are established in this study.

Experimental section

Materials

Tris(pentafluorophenyl)borane (Sigma-Aldrich; purity >95%), benzyl alcohol (Sigma-Aldrich; purity >99.8%), phosphazene base *t*-BuP_4 solution (0.8 M in hexane, Sigma-Aldrich), benzoic acid (Sigma-Aldrich; purity >99.5%), dimethyl sulfoxide (DMSO) (Wako; 99%), *N*,*N*-dimethylformamide (Sigma-Aldrich; 99.8%), and diethyl ether were used as obtained from the manufacturers. Glycidol (Sigma-Aldrich; purity >96%), tetralin (Sigma-Aldrich, 99%), Py (Wako; 99.5%), and TBA (Sigma-Aldrich; ≥98.5%) were dried overnight over calcium hydride and then purified by distillation before use. Toluene (Sigma-Aldrich; ≥99.9%) was passed through purification columns (JCM, JCM-3SPS-SA-6) and bubbled with dry nitrogen gas for more than 15 min, immediately before use.

Ring-opening polymerization procedures using the BCF complex along with N(*n*-Bu)$_3$

Polymerization was carried out using the syringe technique under dry argon baked glass tubes equipped with a three-way stopcock or in sealed glass vials. The typical procedure for glycidol with BCF/TBA is described as follows. First, glycidol (0.67 mL, 10.0 mmol), toluene (2.43 mL), and tetralin (0.30 mL) were sequentially added into a 50 mL round-bottom flask filled with argon, after which the reaction mixture was cooled to 0 °C. In another sealed glass vial, a solution of BCF catalyst (0.58 mL, 25 mM in toluene) was mixed with a solution of N(*n*-Bu)$_3$ (0.14 mL, 400 mM in toluene) for 15 min; subsequently, 0.60 mL of the resultant mixture was transferred to the polymerization mixture with the total volume maintained at 4.00 mL ($[BCF]_0/[TBA]_0$ = 3/12 mM). Immediately after mixing, the reaction mixture was placed in a bath maintained at 100 °C for 6 h. The polymerization was terminated with methanol at various intervals. Monomer conversion was determined by measuring the residual monomer concentration using ^{1}H NMR with tetralin as an internal standard. The quenched solution was decanted and dissolved in DMSO. The polymer solution was precipitated in cold diethyl ether to remove low-molecular-weight oligomers and the remaining catalyst. The final product was vacuum dried at 30 °C overnight (0.68 g, 91% yield) and characterized using SEC (M_n = 1790, M_w/M_n = 1.92).

Ring-opening polymerization procedures using the BCF complex along with pyridine

Polymerization was carried out using the syringe technique under dry argon baked glass tubes equipped with a three-way stopcock or in sealed glass vials. The typical procedure for glycidol with BCF/Py is described as follows. First, glycidol (0.67 mL, 10.0 mmol), toluene (2.31 mL), and tetralin (0.30 mL) were sequentially added into a 50 mL round-bottom flask filled with argon, after which the reaction mixture was cooled to 0 °C. In another sealed glass vial, a solution of BCF catalyst (0.58 mL, 25 mM in toluene) was mixed with a solution of Py (0.29 mL, 100 mM in toluene) for 15 min; subsequently, 0.72 mL of the resultant mixture was transferred to the polymerization mixture with the total volume maintained at 4.00 mL ($[BCF]_0/[Py]_0$ = 3/6 mM). Immediately after mixing, the reaction mixture was placed in a bath maintained at 100 °C for 18 h. The polymerization was terminated with methanol at various intervals. Monomer conversion was determined by measuring the residual monomer concentration using ^{1}H NMR with tetralin as an internal standard. The quenched solution was decanted and dissolved in DMSO. The polymer solution was precipitated in cold diethyl ether to remove low-molecular-weight oligomers and the remaining catalyst. The final product was vacuum dried at 30 °C overnight (0.66 g, 89% yield) and characterized using SEC (M_n = 1370, M_w/M_n = 1.67).

BCF-catalyzed ring-opening polymerization of glycidol

BCF-catalyzed polymerization of glycidol was synthesized by following established procedures.[27]

Synthesis of linear polyglycidol by anionic ring-opening polymerization

Monomer (tetrahydropyranyl glycidyl ether, TGE) was synthesized by following established procedures.[35] Polymerization was carried out using the Schenck line technique under a dry argon baked round-bottom flask equipped with a three-way stopcock. Benzyl alcohol (0.105 g, 0.98 mmol), toluene (7.92 mL), and 1.59 mL of *t*-BuP_4 (0.8 M in hexane, 1.27 mmol) were added into a 50 mL round-bottom flask filled with argon. TGE (5.49 mL, 35.1 mmol) was then added to the solution and the mixture was stirred for 24 h in a bath maintained at 25 °C with the total volume fixed at 15.0 mL. The polymerization was quenched by adding benzoic acid (0.16 g, 1.27 mmol) at 0 °C and polymerized TGE (PTGE) was obtained by precipitation in hexane. The polymer solution was passed through an alumina pad along with CH_2Cl_2 and evaporated. The obtained PTGE was hydrolysed in HCl/MeOH (1.25 M) for 24 h at 25 °C and the reaction mixture was neutralized using potassium carbonate. The mixture was filtered and precipitated in excess cold diethyl ether. The resultant linear polyglycidol was vacuum dried and characterized using SEC (lin-PG in Table 1, target DP_n = 36, M_n = 4420, M_w/M_n = 1.04).

Published on 26 January 2022. Downloaded by Yonsei University on 2/28/2022 1:44:30 AM.

Table 1 Characterization of structure controlled PGs in this work[a,b]

Polymer code	Structure	DB[b]	MALDI-ToF[c] M_n	SEC[d] M_n	SEC[d] M_w/M_n	T_g[e] (°C)
TBA-P15	hb-PG	0.51	2850	1790	1.92	−27
Py-P11	bc-PG	0.48	2730	1370	1.67	−38
Linear PG	lin-PG	0	2660	4420	1.04	−8

[a] The conversion was determined by ^{1}H NMR using tetralin as an internal standard. [b] Degree of branching (DB) was calculated by inverse-gated ^{13}C NMR using the following equation: (D + T)/(D + T + L) (D = dendritic unit; T = terminal unit; L = linear unit). [c] MALDI-ToF mass of the PG homopolymer from 1500 Da to 4500 Da. [d] Measured by size-exclusion chromatography calibrated with PEO standards in DMF (50 mM LiBr, 45 °C, flow rate 1.0 mL min^{-1}). [e] Glass-transition temperature (T_g) was determined by differential scanning calorimetry (DSC) at a rate of 10 °C min^{-1} and the median of that range is considered T_g.

Measurements

The M_n and M_w/M_n of polymers were measured at 45 °C using SEC with dimethylformamide (DMF) as an eluent. For DMF-SEC, three polystyrene-gel columns [KD-802 (from Shodex); pore size, 150 Å; 8 mm i.d. × 300 mm, KD-803 (from Shodex); pore size, 500 Å; 8 mm i.d. × 300 mm, KD-804 (from Shodex); pore size, 1500 Å; 8 mm i.d. × 300 mm] were connected to a PU-4180 pump, an RI-4030 refractive-index detector, and a UV-4075 ultraviolet detector (JASCO); the flow rate was maintained at 1.0 mL min^{-1}. The columns were calibrated against 13 standard poly(ethylene glycol) (PEO) samples (Agilent Technologies; M_p = 980–811 500; M_w/M_n = 1.03–1.11) to analyse the obtained PG samples. ^{1}H NMR was performed on a Bruker Ultrashield spectrometer operating at 300 MHz. ^{1}H NMR (400 MHz), ^{13}C NMR (100 MHz), and ^{11}B (128 MHz) spectra were obtained using an AVANCE III HD NMR spectrometer (Bruker). All spectra were recorded in ppm units using deuterated solvents DMSO-d_6 and toluene-d_8 at room temperature. ^{1}H diffusion-ordered spectroscopy (DOSY) was performed at 25 °C on an Agilent DD2 600 MHz NMR spectrometer, after dissolving the sample in DMSO-d_6. Matrix-assisted laser desorption/ionization time-of-flight (MALDI-ToF) analysis was performed using an Ultraflex III MALDI mass spectrometer; 2,5-dihydroxybenzoic acid was used as the matrix. Differential scanning calorimetry (DSC) was conducted on polymer samples under a dry nitrogen flow at a heating or cooling rate of 10 °C min^{-1} on a Q2000 calorimeter (TA Instruments).

^{1}H DOSY NMR experiments

Three samples (TBA-P15, Py-P11, and linear PG) were separately prepared at a concentration of 24 mg mL^{-1} in dried DMSO-d_6. For diffusion measurements, pulsed-field-gradient DOSY NMR experiments were performed with a maximum gradient of 52.9 mT m^{-1}. In order to avoid the influence of convection on the bulk solution during the diffusion measurements, a bipolar-pulse pair stimulated echo sequence with convection compensation was used, which comprises a double simulated echo sequence with bipolar gradients. The pulse sequences contained a 0.5 ms delay to stabilize the gradients. The magnetic field gradient amplitudes were gradually increased from 2.10 × 10^{-2} up to 5.2 × 10^{-1} T m^{-1} for the maximum gradient strength in a linear ramp. For each gradient amplitude, 15 transients of 16 384 complex data points were obtained for a total experimental time of 12 min. The diffusion gradient length (δ) of 2 ms was selected for the diffusion time, with a diffusion delay of 20 ms. The NMR data were processed, and the diffusion coefficients (D) were determined using the DOSY Toolbox software package. Errors of approximately 1.8% were obtained for the diffusion experiments. The main source of error in the diffusion experiments was the reproducibility of data acquisition. The signal decay caused by gradients was obtained by DOSY fitting of the Stejskal–Tanner equation:

$$S = S_0 \exp(-D\gamma^2 g^2 \delta^2 (\Delta - \delta/3))$$

where S is the signal amplitude as a function of gradient strength g, S_0 is the signal amplitude at g = 0, D is the diffusion coefficient, γ is the proton gyromagnetic ratio, δ is the gradient pulse duration, and Δ is the diffusion time.

Results and discussion

Initiation of frustrated Lewis pairs and the mechanism of ring-opening polymerization

BCF is a powerful Lewis acid catalyst because of its electron-withdrawing nature and the steric bulkiness of its three pentafluorinated aryl rings. Therefore, it can form FLPs with organic Lewis bases. Considering these features, organic Lewis bases such as TBA and Py were selected to form FLPs with BCF for the polymerization of glycidol, which might affect the propagation mechanism and the polymerization reactivity. For example, the formation of FLPs between the BCF catalyst and a base at early stages can lead to a reduced catalytic reactivity for the polymerization. In addition, the Lewis base can undergo H-bonding with the hydroxyl group of glycidol, which might favour the AM mechanism because of the increase in the nucleophilicity of oxygen in the hydroxyl group. Therefore, these FLPs are expected to govern the structure of the PG.

In order to study the catalytic patterns of FLPs, BCF was mixed with TBA to generate the corresponding FLP, and the resultant mixture was analysed by *in situ* ^{1}H and ^{11}B NMR: $[BCF]_0/[TBA]_0$ = 20/40 mM (Fig. S1†). Upon mixing, the peaks attributed to free TBA were clearly shifted to higher toluene concentrations in the NMR spectra recorded at 25 °C, indicating that the FLP was successfully formed. Moreover, under thermal conditions (80 °C), the peaks attributed to the BCF-TBA Lewis pair were shifted to downfield because of the formation of a loose BCF–TBA Lewis pair.

Before applying the FLP catalytic system to the polymerization, glycidol was mixed with the BCF-TBA Lewis pair to investigate the catalytic reactivity for ring-opening polymerization: $[GD]_0/[BCF]_0/[TBA]_0$ = 40/20/40 mM (Fig. 1). The peak

 This journal is © The Royal Society of Chemistry 2022

Published on 26 January 2022. Downloaded by Yonsei University on 2/28/2022 1:44:30 AM.

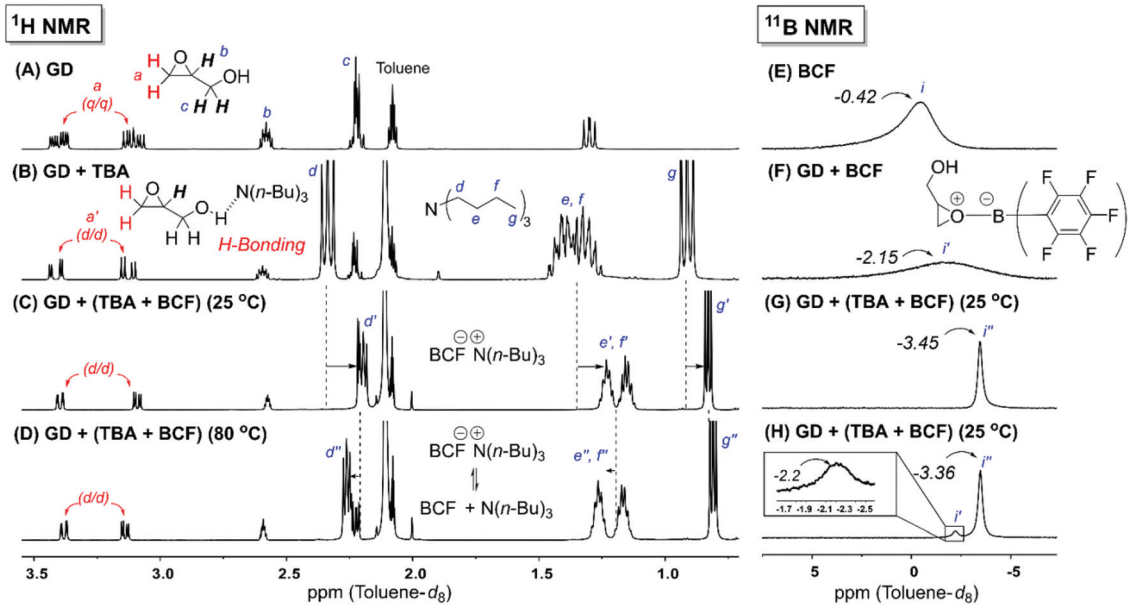

Fig. 1 ^{1}H NMR spectra of (A) ($[GD]_0$ = 40 mM in toluene) at 25 °C, (B) a mixture of GD and TBA at a 1 : 1 ratio ($[GD]_0$ = 40 mM; $[TBA]_0$ = 40 mM) at 25 °C, (C) a mixture of GD and BCF-TBA ($[GD]_0$ = 40 mM; $[TBA]_0$ = 40 mM; $[BCF]_0$ = 20 mM) at 25 °C, and (D) a mixture of GD and BCF-TBA ($[GD]_0$ = 40 mM; $[TBA]_0$ = 40 mM; $[BCF]_0$ = 20 mM) at 80 °C; ^{11}B NMR spectra of (E) BCF ($[BCF]_0$ = 20 mM) at 25 °C, (F) a mixture of GD and BCF with a 2 : 1 ratio ($[GD]_0$ = 40 mM; $[BCF]_0$ = 20 mM) at 25 °C, (G) a mixture of GD and BCF-TBA ($[GD]_0$ = 40 mM; $[TBA]_0$ = 40 mM; $[BCF]_0$ = 20 mM) at 25 °C, and (H) a mixture of GD and BCF-TBA ($[GD]_0$ = 40 mM; $[TBA]_0$ = 40 mM; $[BCF]_0$ = 20 mM) at 25 °C after polymerization at 80 °C for 3 h.

signal for epoxide in an equimolar mixture of glycidol and TBA (*a′*; 3.45–3.09 ppm; doublet of doublets; Fig. 1B) was obviously different from that of only epoxide (*a*; 3.45–3.06 ppm; quartet of quartets; Fig. 1A) because of the H-bonding between the hydroxyl group of the glycidol and the nitrogen atom of TBA. As shown in Fig. 1C, polymerization of glycidol did not occur in the presence of the BCF-TBA Lewis pair because of the reduced catalytic reactivity resulting from the formation of the Lewis pair and the H-bonding of the excess TBA with glycidol. Although a dynamic equilibrium between tight and loose (or dissociated) BCF-TBA Lewis pairs was observed at higher temperatures, H-bonding between glycidol and excess TBA still occurred (Fig. 1D). However, a mixture of BCF and glycidol immediately formed a zwitterionic intermediate, which yielded a broad peak at −2.15 ppm in the ^{11}B NMR spectrum (*i′*; Fig. 1F). The formation of a zwitterion between BCF and glycidol in the mixture of glycidol and BCF-TBA Lewis pairs was observed after heating at 80 °C for 3 h. The formation of this zwitterion is likely attributed to the formation of loose BCF-TBA Lewis pairs or by their dissociation at high temperatures, which results in the formation of a zwitterionic intermediate with glycidol to drive propagation (*i′*; −2.20 ppm; Fig. 1H).

Similarly, Py was also used as a Lewis base to determine the catalytic pattern of the Lewis pair with BCF, compared to that of the BCF-TBA Lewis pair because of its reduced steric effect. In the model system, BCF-Py exhibited a similar catalytic pattern, indicating the successful formation of the BCF–glycidol zwitterion, while excess Py still interacts with the hydroxyl group of glycidol at high temperatures (Fig. S2 and S3†).

Based on these results, we propose a possible ring-opening polymerization mechanism of glycidol (Scheme 2).[36] In this catalytic system, stable FLPs are formed between the BCF catalyst and organic bases at an early stage. When the temperature is increased, a loose or dissociated Lewis pair is formed by recovering the Lewis acidity of BCF. The glycidol monomer is activated by the formation of a zwitterionic intermediate. Propagation then occurs by a nucleophilic attack of the glycidol, which follows the competition between the ACE and AM mechanisms. Of these, the AM mechanism was more preferred than the ACE mechanism because of H-bonding between the Lewis base and the glycidol with increased nucleophilicity. Finally, the polymerization was terminated by the release of separated Lewis pairs.

Structural control of polymer topologies and terminal groups by FLP-catalyzed ring-opening polymerization

Based on the previously discussed NMR analyses of Lewis pairs, BCF was examined for the polymerization of glycidol along with varying molar ratios of Lewis bases at different polymerization temperatures (Tables S1 and S2†). Both FLP-catalyzed polymerizations demonstrated much slower kinetics than BCF itself because of the formation of stable FLPs at the early stage. Moreover, higher concentrations of Lewis base and increased reaction temperatures in the polymerization system were observed to enhance the monomer conversion and polymerization rate (Fig. 2A). In particular, polymerizations using FLP systems induced interesting structural changes with a higher DB as well as changes in structural units, including $L_{1,3}$, $L_{1,4}$, D, T_1, and T_2 (Fig. S4 and Tables S3–S6†).

Published on 26 January 2022. Downloaded by Yonsei University on 2/28/2022 1:44:30 AM.

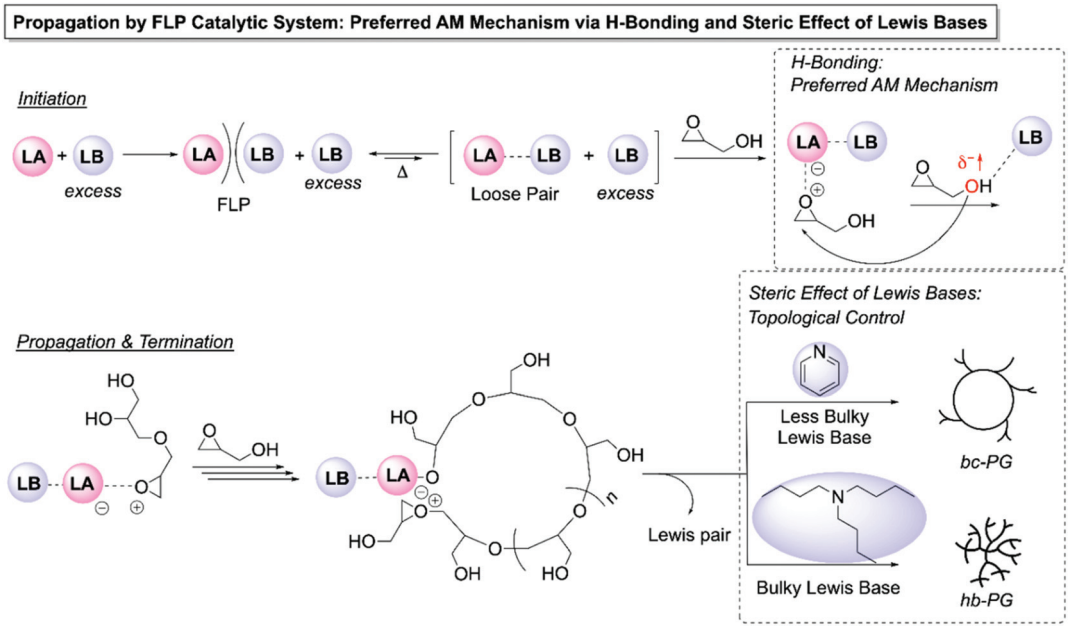

Scheme 2 Proposed mechanism for FLP-catalyzed polymerization of glycidol and topological control of PGs by the steric effect of organic bases in FLP catalysts.

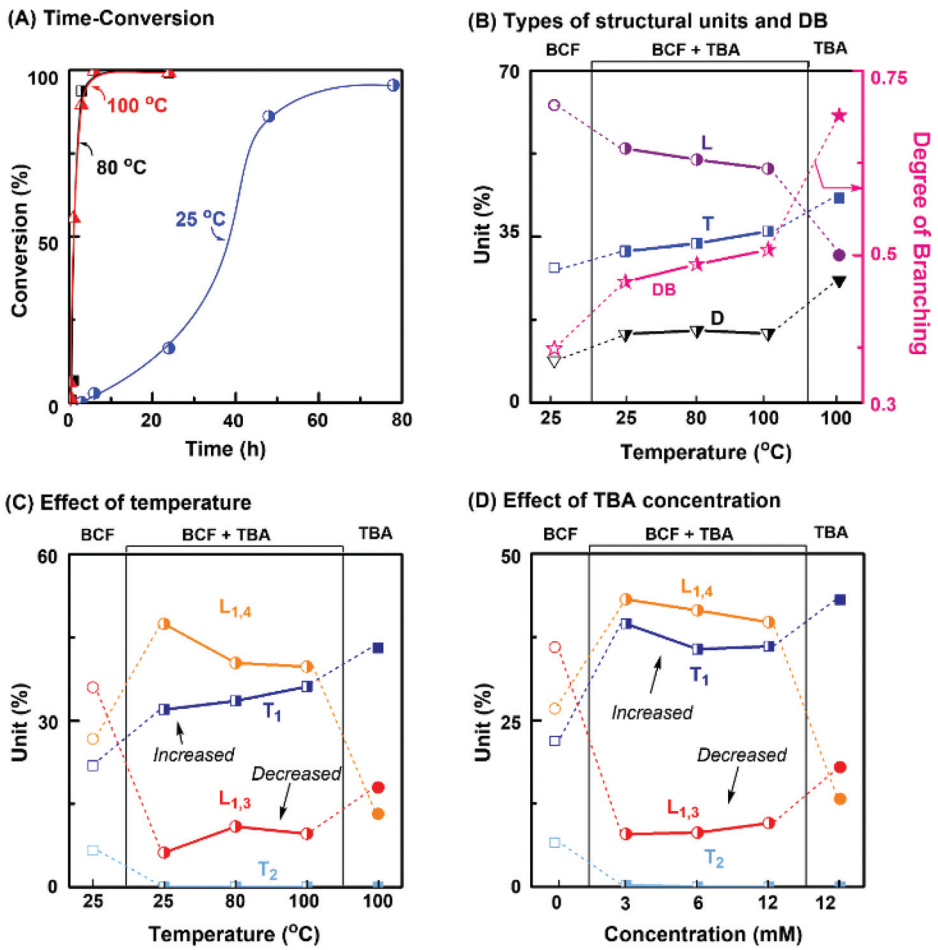

Fig. 2 BCF-TBA Lewis pair-catalyzed polymerization of glycidol and detailed tracking of the structural changes in the PG chain: (A–C) $[GD]_0$ = 2500 mM; $[BCF]_0$ = 3 mM; $[TBA]_0$ = 12 mM in toluene, and (D) $[GD]_0$ = 2500 mM; $[BCF]_0$ = 3 mM; $[TBA]_0$ = 3, 6, or 12 mM in toluene.

 This journal is © The Royal Society of Chemistry 2022

Published on 26 January 2022. Downloaded by Yonsei University on 2/28/2022 1:44:30 AM.

Specifically, although changes in the overall compositions of the respective units (*i.e.*, L, D, and T) were negligible in the polymer chain, the detailed compositions of $L_{1,4}$ and T_1 groups containing secondary alcohols increased clearly, while those of $L_{1,3}$ and T_2 groups containing primary alcohols decreased compared with that of an only BCF system.[27] In addition, the system catalyzed only with a Lewis base displayed clear differences in the detailed PG composition (Fig. 2B–D).

These results suggest that FLP-catalyzed polymerization follows a different propagation mechanism, indicating that a dissociated Lewis base from the FLP and/or an excess Lewis base can undergo H-bonding with the hydroxyl group of the monomer, thereby favouring the AM mechanism because of increased nucleophilicity. Analogously, polymerization catalyzed by BCF with either TBA or Py in a form of FLP demonstrated a similar preference for the AM mechanism involving H-bonding over the ACE mechanism. Interestingly, however, MALDI-ToF spectrometry revealed different topologies of the resulting PGs depending on the type of Lewis base.[22,26,37,38] For example, the MALDI-ToF spectrum of TBA-P15, which was prepared using the BCF-TBA system, shows regularly spaced peaks with a mass interval corresponding to glycidol (74.04) (blue triangle in Fig. 3A and Fig. S5†). The absolute *m*/*z* value of 2558.66 corresponds to a hyperbranched PG chain, which has a higher molecular weight than the branched cyclic structure with an additional water molecule ([34 GD units + H_2O + Na^+]). In fact, the BCF-Py system yielded a PG with a fully branched cyclic structure (pink circle in Fig. 3B, observed *m*/*z*: 2540.59; [34 GD units + Na^+]). These results were attributed to the difference in the steric effects of the different Lewis bases, which may prevent the formation of stable zwitterionic intermediates during propagation (Scheme 2).

As a control, a linear structure with a similar molecular weight was prepared by anionic ring opening polymerization

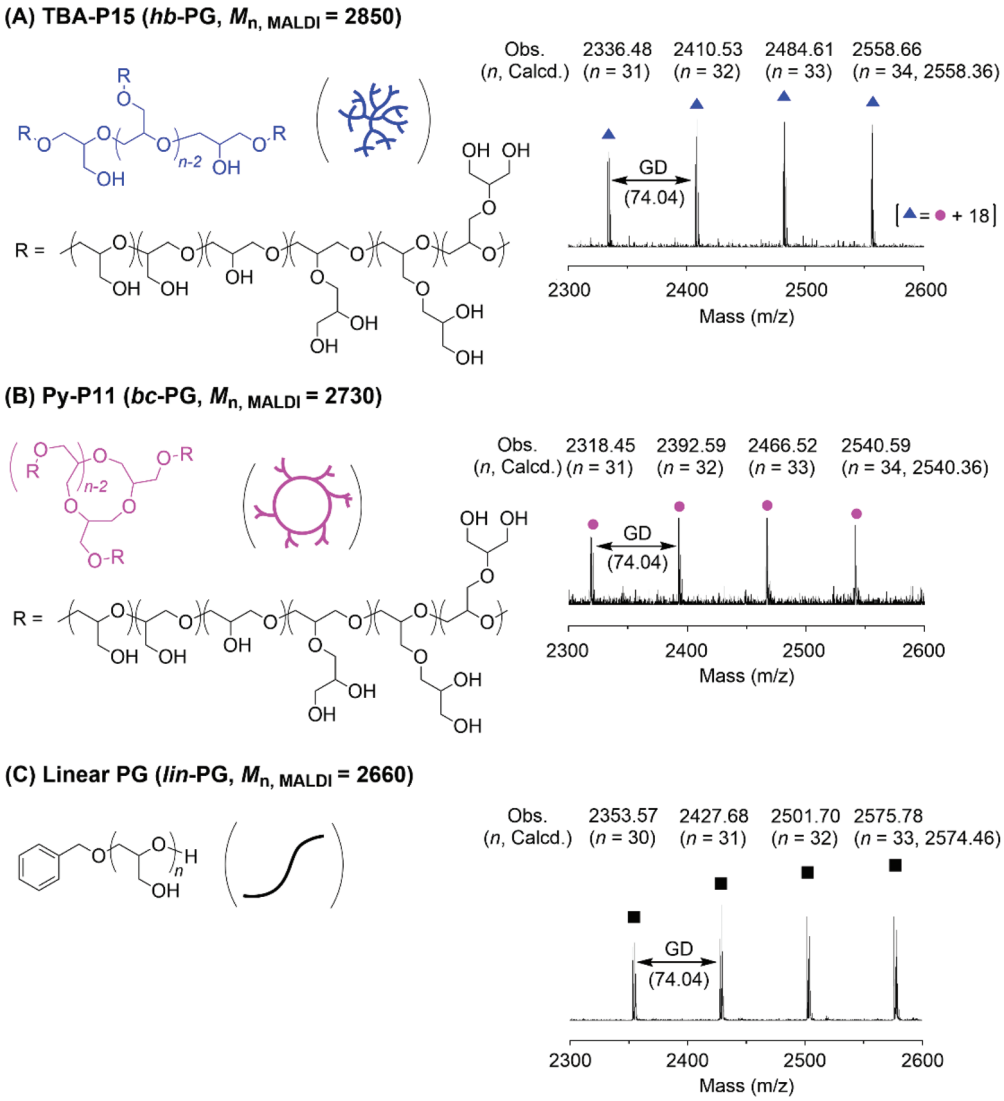

Fig. 3 A representative MALDI-ToF spectrum for (A) TBA-P15 (hb-PG), (B) Py-P11 (bc-PG), and (C) linear PG (lin-PG) from 2300 to 2600 Da with individual peak assignments.

Published on 26 January 2022. Downloaded by Yonsei University on 2/28/2022 1:44:30 AM.

using benzyl alcohol as an initiator with tetrahydropyranyl glycidyl ether (TGE), which is a protected glycidol derivative developed by our group.[33] After acid hydrolysis of the protecting group in the polymer chain, the linear PG was successfully obtained and characterized using ^{1}H NMR and MALDI-ToF (Fig. S6† and black square in Fig. 3C, observed *m*/*z*: 2575.78; [benzyl alcohol initiator (108.14) + 33 GD units + Na^+]).

Correlation between polymer topology and the bulk and solution states

In order to study the effect of the different polymer structures with similar degrees of polymerization on the PG chains, three polymer samples with similar molecular weights were subjected to thermal analysis using DSC (Table 1 and Fig. S7;† TBA-P15, hb-PG, $M_{n,MALDI}$ = 2850, M_w/M_n = 1.06; Py-P11, bc-PG, $M_{n,MALDI}$ = 2730, M_w/M_n = 1.08; linear PG, lin-PG, $M_{n,MALDI}$ = 2660, M_w/M_n = 1.01). Interestingly, characteristic glass-transition temperatures (T_g) were observed for different polymer topologies. As expected, lin-PG exhibited the highest T_g, whereas bc-PG structures exhibited the lowest T_g; hb-PG exhibited an intermediate T_g (Table 1 and Fig. S7;† $T_{g,lin\text{-}PG}$ = −8 °C, $T_{g,TBA\text{-}P15}$ = −27 °C, and $T_{g,Py\text{-}P11}$ = −38 °C). The different polymer topologies appear to affect the intra- and inter-molecular H-bonding between polymer chains, which lead to different T_g values.[20] Although these topologically controlled PGs had similar DB values (similar number of chain ends and number of branch points) and molecular weights (similar number of H-bonds), intermolecular or intramolecular H-bonding in PGs is considerably influenced by the polymeric topology. Further research is currently underway to ascertain the relationship between polymer topologies and physical properties using broader sample sets with different molecular weight ranges.

As discussed in the preceding section, polymers with different topologies and similar molecular weights exhibited interesting phenomena in their bulk states. Furthermore, to investigate the effect of different polymer topologies in solution, diffusion coefficients (D) were determined using ^{1}H DOSY. The diffusion coefficient of a fluid characterizes its random Brownian motion and provides information about the size and morphology of the molecules in the fluid environment.[39] Fig. 4 shows the dependence of diffusion coefficients on the DB values of the topology-controlled PGs at similar absolute molecular weights ($M_{n,MALDI}$) (Fig. S8–S11†).

The diffusion coefficient of the branched cyclic polymer ($D_{Py\text{-}P11}$ = 5.98 ± 0.20 [10^{-10} m s^{-2}]) was substantially greater than those of the linear-type polymers ($D_{TBA\text{-}P15}$ = 4.34 ± 0.10 [10^{-10} m s^{-2}] and $D_{lin\text{-}PG}$ = 3.69 ± 0.12 [10^{-10} m s^{-2}]). In particular, the diffusion coefficient of Py-P11 (DB = 0.48) was greater than that of TBA-P15 (DB = 0.51), which has a similar DB but different polymer topologies; this result indicates that the cyclic polymer yields a more compact coil conformation compared to its linear counterpart because of a lower conformational degree of freedom originating from the absence of polymer chain ends. Remarkably, the diffusion coefficient of hb-PG with a higher DB value, TBA-P15, was greater than that of lin-PG (DB = 0). This result is likely caused by the reduction in chain mobility resulting from the decreased branching of the polymer chains. In addition, given the limited molecular weight of the polymers, we did not observe any dependence on their solubility with respect to the topologies.

In parallel, the correlation between polymer structures and their solution behaviours was further examined through SEC analyses. The relative molecular weights determined using SEC analysis and the diffusion coefficients depend on the hydrodynamic volume of the polymer in solution. Therefore, DMF-SEC analyses were employed to determine the relative molecular weights of the obtained PGs with different topologies. This could indirectly relate hydrodynamic volume changes with the diffusion coefficients determined by ^{1}H DOSY (Fig. 4C, Table 1, and Fig. S12†). Interestingly, the relative molecular weights ($M_{n,SEC}$) obtained from the SEC curves were different for the different PGs; these results were well-correlated with the estimated hydrodynamic volume determined from D values for each polymer structure. These results suggest the importance of DB control in tuning the polymer properties and achieving topological control in macromolecular architectures.

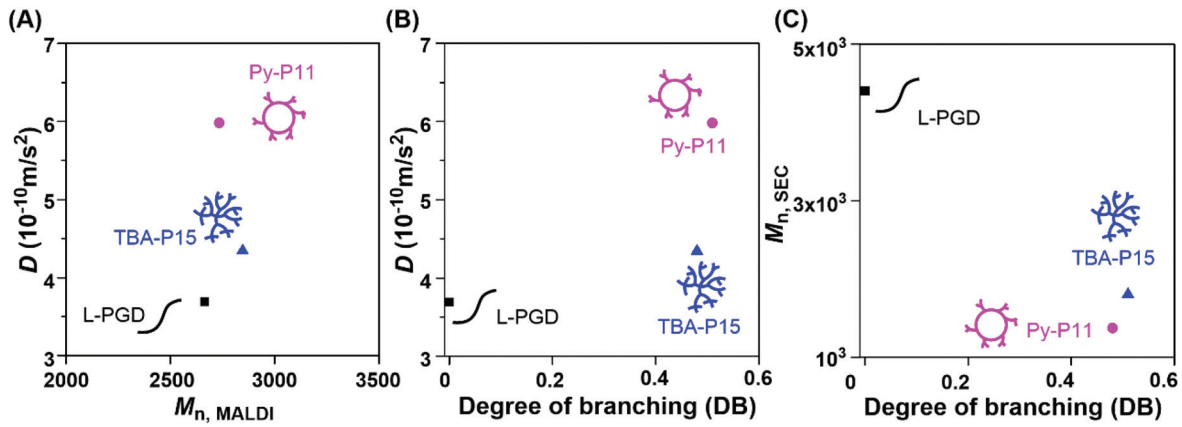

Fig. 4 Correlation between polymer structures and solution behaviours. (A) Dependence of diffusion coefficients on the absolute molecular weight and (B) DB values, and (C) dependence of relative molecular weights ($M_{n,SEC}$) on the DB values.

This journal is © The Royal Society of Chemistry 2022

Published on 26 January 2022. Downloaded by Yonsei University on 2/28/2022 1:44:30 AM.

Conclusions

A combination of TBA or Py with the BCF catalyst in the polymerization system not only favoured the AM mechanism because of hydrogen bonding with the hydroxyl group of glycidol, but also provided different polymer topologies by forming FLPs. In particular, the less-hindered base Py yielded the perfect branched cyclic polymer with increased DB values, whereas the sterically hindered base, TBA, yielded completely hyperbranched PGs, as confirmed by ^{1}H NMR, inverse-gated ^{13}C NMR analyses, and MALDI-ToF. Further analyses such as DSC, ^{1}H DOSY, and SEC were used to examine the unique physical features of the obtained PGs in the bulk and solution states as well as their wide structural variety with different topologies. Altogether, these results supported a significant correlation between the topologies and physical properties of the polymers. We anticipate that FLP-catalyzed polymerization will unravel more intriguing examples involving highly controlled polymer topologies for challenging applications.

Author contributions

The manuscript was written through the contribution of all authors. All authors have given approval to the final version of the manuscript. S. E. K.: experimentation, analysis, and writing; Y.-R. L.: DOSY experimentation and analysis; M. K. and E. S.: experimentation and analysis; H.-J. P., J. C. K., and J.-E. J.: analysis; Y. I. P.: conceptualization and supervision; B.-S. K. and S.-H. L.: conceptualization, supervision, and editing.

Conflicts of interest

There are no conflicts to declare.

Acknowledgements

We thank Dr Kyung-Youl Baek of the Korea Institute of Science and Technology (KIST) for his insights into ^{1}H DOSY NMR spectra. This study was supported by the Ministry of Trade, Industry & Energy (MOTIE, Korea) under the Industrial Technology Innovation Program (No. 20011123) and the Korea Research Institute of Chemical Technology (KRICT) (No. KS2041-00). This work was also supported by the National Research Foundation of Korea (NRF-2021R1A2C3004978).

Notes and references

1 K. Matyjaszewski and N. V. Tsarevsky, *J. Am. Chem. Soc.*, 2014, **136**, 6513–6533.
2 S. E. Seo and C. J. Hawker, *Macromolecules*, 2020, **53**, 3257–3261.
3 D. A. Tomalia, H. Baker, J. Dewald, M. Hall, G. Kallos, S. Martin, J. Roeck, J. Ryder and P. Smith, *Macromolecules*, 1986, **19**, 2466–2468.
4 C. J. Hawker and J. M. J. Frechet, *J. Am. Chem. Soc.*, 1990, **112**, 7638–7647.
5 X. Feng, D. Taton, E. Ibarboure, E. L. Chaikof and Y. Gnanou, *J. Am. Chem. Soc.*, 2008, **130**, 11662–11676.
6 E. Östmark, S. Harrisson, K. L. Wooley and E. E. Malmström, *Biomacromolecules*, 2007, **8**, 1138–1148.
7 C. Feng, Y. Li, D. Yang, J. Hu, X. Zhang and X. Huang, *Chem. Soc. Rev.*, 2011, **40**, 1282–1295.
8 B. I. Voit and A. Lederer, *Chem. Rev.*, 2009, **109**, 5924–5973.
9 R. A. Shenoi, J. K. Narayanannair, J. L. Hamilton, B. F. L. Lai, S. Horte, R. K. Kainthan, J. P. Varghese, K. G. Rajeev, M. Manoharan and J. N. Kizhakkedathu, *J. Am. Chem. Soc.*, 2012, **134**, 14945–14957.
10 B. A. Laurent and S. M. Grayson, *Chem. Soc. Rev.*, 2009, **38**, 2202–2213.
11 A. Blencowe and G. G. Qiao, *J. Am. Chem. Soc.*, 2013, **135**, 5717–5725.
12 D. Wilms, S.-E. Stiriba and H. Frey, *Acc. Chem. Res.*, 2010, **43**, 129–141.
13 A. Sunder, R. Hanselmann, H. Frey and R. Mülhaupt, *Macromolecules*, 1999, **32**, 4240–4246.
14 R. Tokar, P. Kubisa, S. Penczek and A. Dworak, *Macromolecules*, 1994, **27**, 320–322.
15 S.-E. Stiriba, H. Kautz and H. Frey, *J. Am. Chem. Soc.*, 2002, **124**, 9698–9699.
16 S. Song, J. Lee, S. Kweon, J. Song, K. Kim and B.-S. Kim, *Biomacromolecules*, 2016, **17**, 3632–3639.
17 S. Son, E. Shin and B.-S. Kim, *Macromolecules*, 2015, **48**, 600–609.
18 Y. Segawa, T. Higashihara and M. Ueda, *J. Am. Chem. Soc.*, 2010, **132**, 11000–11001.
19 T. Higashihara, Y. Segawa, W. Sinananwanich and M. Ueda, *Polym. J.*, 2012, **44**, 14–29.
20 C. Schubert, M. Schömer, M. Steube, S. Decker, C. Friedrich and H. Frey, *Macromol. Chem. Phys.*, 2018, **219**, 1700376.
21 M. Dadkhah, H. Shamlooei, E. Mohammadifar and M. Adeli, *RSC Adv.*, 2018, **8**, 217–221.
22 I. Asenjo-Sanz, A. Veloso, J. I. Miranda, A. Alegría, J. A. Pomposo and F. Barroso-Bujans, *Macromolecules*, 2015, **48**, 1664–1672.
23 E. Mohammadifar, A. Bodaghi, A. Dadkhahtehrani, A. Nemati Kharat, M. Adeli and R. Haag, *ACS Macro Lett.*, 2017, **6**, 35–40.
24 C. H. Tran, M. W. Lee, S. A. Kim, H. B. Jang and I. Kim, *Macromolecules*, 2020, **53**, 2051–2060.
25 B. R. Spears, M. A. Marin, J. R. Montenegro-Burke, B. C. Evans, J. McLean and E. Harth, *Macromolecules*, 2016, **49**, 2022–2027.
26 I. Asenjo-Sanz, A. Veloso, J. I. Miranda, J. A. Pomposo and F. Barroso-Bujans, *Polym. Chem.*, 2014, **5**, 6905–6908.

Published on 26 January 2022. Downloaded by Yonsei University on 2/28/2022 1:44:30 AM.

27 S. E. Kim, H. J. Yang, S. Choi, E. Hwang, M. Kim, H.-J. Paik, J.-E. Jeong, Y. I. Park, J. C. Kim, B.-S. Kim and S.-H. Lee, *Green Chem.*, 2022, **24**, 251–258.
28 D. W. Stephan, *Acc. Chem. Res.*, 2015, **48**, 306–316.
29 D. W. Stephan, *J. Am. Chem. Soc.*, 2015, **137**, 10018–10032.
30 M. Hong, J. Chen and E. Y. Chen, *Chem. Rev.*, 2018, **118**, 10551–10616.
31 X.-Q. Li, B. Wang, H.-Y. Ji and Y.-S. Li, *Catal. Sci. Technol.*, 2016, **6**, 7763–7772.
32 S. Aoshima and S. Kanaoka, *Chem. Rev.*, 2009, **109**, 5245–5287.
33 A. Kanazawa, S. Kanaoka and S. Aoshima, *Chem. Lett.*, 2010, **39**, 1232–1237.
34 G.-G. Gu, L.-Y. Wang, R. Zhang, T.-J. Yue, B.-H. Ren and W.-M. Ren, *Polym. Chem.*, 2021, **12**, 6436–6443.
35 J. Song, L. Palanikumar, Y. Choi, I. Kim, T.-Y. Heo, E. Ahn, S.-H. Choi, E. Lee, Y. Shibasaki, J.-H. Ryu and B.-S. Kim, *Polym. Chem.*, 2017, **8**, 7119–7132.
36 M. L. McGraw and E. Y. X. Chen, *Macromolecules*, 2020, **53**, 6102–6122.
37 J. Liu, R. S. Loewe and R. D. McCullough, *Macromolecules*, 1999, **32**, 5777–5785.
38 F. M. Haque, C. R. M. Schexnayder, J. M. Matxain, F. Barroso-Bujans and S. M. Grayson, *Macromolecules*, 2019, **52**, 6369–6381.
39 P. Groves, *Polym. Chem.*, 2017, **8**, 6700–6708.

 This journal is © The Royal Society of Chemistry 2022